Slaby, C.; Könies, A.; Kleiber, R.; Akaslompolo, S.; Kontula, J.

Parametric study of fast-ion-driven modes in Wendelstein 7-X

Published in:
Journal of Physics: Conference Series

DOI:
10.1088/1742-6596/1125/1/012019

Published: 23/11/2018

Document Version
Publisher's PDF, also known as Version of record

Parametric study of fast-ion-driven modes in Wendelstein 7-X

To cite this article: C Slaby *et al* 2018 *J. Phys.: Conf. Ser.* **1125** 012019

IOP Conf. Series: Journal of Physics: Conf. Series **1125** (2018) 012019 doi:10.1088/1742-6596/1125/1/012019

Parametric study of fast-ion-driven modes in Wendelstein 7-X

C Slaby[1], A Könies[1], R Kleiber[1], S Äkäslompolo[1] and J Kontula[2]

[1] Max-Planck-Institut für Plasmaphysik, Greifswald, Germany
[2] Aalto University, Aalto, Finland

E-mail: christoph.slaby@ipp.mpg.de

Abstract. In the 2018 experimental campaign, fast ions in the stellarator Wendelstein 7-X will be generated by neutral beam injection. Later operation phases will also include ion cyclotron resonance heating. The fast ions may excite instabilities in the plasma which can lead to enhanced fast-ion transport and can, in severe cases, cause damage to plasma-facing components.

We present a numerical study of fast-ion-driven Alfvén eigenmodes in a Wendelstein 7-X high-mirror equilibrium. Realistic fast-ion parameters are obtained using the ASCOT code. To model the instabilities, we use the CKA-EUTERPE code package. This model is perturbative, since a fixed mode structure – computed by the ideal-MHD code CKA – is used throughout the calculation. The non-linear gyro-kinetic code EUTERPE computes the power transfer from the fast particles to the mode which defines the growth rate of the instability.

We show that having a fast-ion collision operator present in the simulations is required to accurately predict the non-linear saturation level of the mode. The scaling of the saturated amplitude with respect to fast-ion drag and the pitch-angle collision frequency is investigated and found to vary for different Alfvén eigenmodes.

Furthermore, we study the impact of several other actuators that might be of experimental relevance for finding operation windows that show Alfvén-eigenmode activity. Examples are the effects of a radial electric field and the composition of the background plasma (hydrogen versus helium). While growth rates are found to be reduced in helium plasmas, including a radial electric field, typically present in Wendelstein 7-X, seems to have little influence on the modes.

1. Introduction

The 2018 experimental campaign of Wendelstein 7-X (W7-X), for the first time, includes neutral beam injection (NBI). This system supplies energetic ions, which heat the plasma via collisional energy exchange. The fast ions thermalize and eventually become part of the background plasma, thus contributing to fuelling. While slowing down, the parallel velocity of a fast ion can become resonant with the phase velocity of Alfvén eigenmodes (AEs) present in the plasma. In that case a resonant transfer of energy from the fast ion to the mode takes place [1]. The mode can grow in amplitude and influence the particle trajectories. This re-distribution of highly energetic ions could potentially damage the device [2].

A number of AEs, and their possible destabilization by fast ions, was recently investigated [3] (see that reference for details). We used a realistic fast-ion density profile and a slowing-down distribution function in energy space, both calculated by the ASCOT code [4, 5] for plasma parameters expected for the 2018 experimental campaign. While Ref. [3] reported on first

results, we now aim to investigate further effects and possible experimental actuators that could influence the non-linear behaviour of the modes.

Firstly, we will describe the CKA-EUTERPE model used for the simulations. Secondly, we will investigate the wave-particle power transfer in phase space and compare the linear growth rates of the modes in hydrogen and helium plasmas. We will then study the effects of pitch-angle collisions and fast-ion drag on the non-linear saturation. Furthermore we investigate the effects of a radial electric field on the mode evolution, with emphasis on the non-linear phase. Finally, conclusions will be drawn.

2. The CKA-EUTERPE model

The CKA-EUTERPE code package [6] has recently been described in detail in Ref. [7]. For the sake of brevity, only the key aspects are repeated here.

CKA-EUTERPE combines the ideal-MHD eigenvalue code CKA and the global non-linear gyro-kinetic particle-in-cell code EUTERPE. A spatial mode structure and frequency are calculated using CKA by solving the eigenvalue problem

$$\omega^2 D_2 \phi_0 (\mathbf{r}) = D_1 \phi_0 (\mathbf{r}) \tag{1}$$

with linear differential operators D_1 and D_2 defined in Refs. [6, 7]. ω_0 and ϕ_0 denote the mode frequency and its electrostatic potential (spatial part), respectively. $\mathbf{r}$ is the spatial position. Since ideal-MHD theory is employed, we can use the fact that the parallel electric field has to vanish in order to determine the vector potential

$$A_{\parallel,0} = \frac{\mathrm{i}}{\omega} \mathbf{b} \cdot \nabla \phi_0, \tag{2}$$

where $\mathbf{b}$ is a unit vector tangent to the background magnetic field.

ϕ_0, $A_{\parallel,0}$, and ω are given to EUTERPE, which solves the gyro-kinetic equation

$$\frac{\partial f}{\partial t} + \dot{\mathbf{R}} \cdot \nabla f + \dot{v}_\parallel \frac{\partial f}{\partial v_\parallel} + \dot{\mu} \frac{\partial f}{\partial \mu} = \mathcal{C} (f) \tag{3}$$

for the distribution function f of the fast particles (if the species index is omitted, fast ions are meant) moving in the external magnetic field as well as in the self-excited electromagnetic fields. Thus, the model is non-linear. The right-hand side of the kinetic equation includes a collision operator, which will be specified below. μ is the specific magnetic moment defined as $\mu = v_\perp^2/(2B)$. The distribution function is split, $f = f^{(0)} + f^{(1)}$, with $f^{(0)}$ being the slowing-down distribution function of the fast ions and $f^{(1)}$ denoting the perturbation.

In the framework of CKA-EUTERPE no field equations need to be solved. The fast ions simply contribute to a time-dependent power transfer (see below), which is used to calculate the time development of the mode with a fixed spatial structure. Therefore, we can use the so-called $v_\parallel$-formulation of gyro-kinetic theory. The corresponding equations of motion for the marker particles can be found in Ref. [7].

Note that in the CKA-EUTERPE model the mode structure remains fixed, and only a complex amplitude is allowed to evolve in time. Thus, the model is perturbative and cannot capture fast-ion-induced mode structure modifications, but is much faster and more stable than fully gyro-kinetic approaches. The equations for the amplitudes of the electromagnetic potentials (denoted by a hat symbol) are

$$\frac{\partial \hat{\phi}}{\partial t} = \mathrm{i}\omega \left(\hat{A}_\parallel - \hat{\phi} \right) + 2 \left(\gamma (t) - \gamma_\mathrm{d} \right) \hat{\phi} \qquad \text{and} \qquad \frac{\partial \hat{A}_\parallel}{\partial t} = \mathrm{i}\omega \left(\hat{\phi} - \hat{A}_\parallel \right). \tag{4}$$

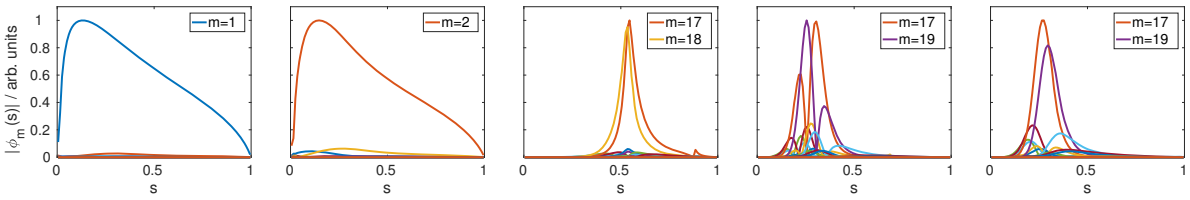

Figure 1. A selection of modes found by CKA. From left to right: $(m = 1/n = -1)$ GAE, $(m = 2/n = -2)$ GAE, $(m = 17, 18/n = -16)$ TAE, $(m = 17, 19/n = -16)$ EAE (even), $(m = 17, 19/n = -16)$ EAE (odd). s is the normalized toroidal flux. Reproduced from Ref. [3].

They are derived from the quasi-neutrality equation – describing the background plasma with MHD theory and the fast ions gyro-kinetically – and Ampère's law. Ref. [8] will describe the details of the model. The frequency of the mode may change as long as $\delta\omega/\omega \ll 1$ is fulfilled. This separation of time scales, where the oscillation of the mode is faster than the evolution of the amplitudes, has been used in the derivation of Eqs. (4). The time-dependent growth rate $\gamma(t) = T(t)/(2W)$ is defined as the quotient of the resonant wave-particle power transfer

$$T(t) = -\int \mathrm{d}\Gamma\ B_{\parallel}^{\star}\left[\frac{m}{ZeB}\mathbf{b}\times\left(v_{\parallel}^{2}\boldsymbol{\kappa}+\mu\nabla B\right)\cdot\left(Ze\nabla_{\perp}\phi^{*}(\mathbf{r},t)\,f^{(1)}\right)\right] \tag{5}$$

and the wave energy

$$W = \int \mathrm{d}^3 r\ \frac{\rho}{B^2}\left|\nabla_{\perp}\phi\right|^2. \tag{6}$$

The notation is conventional: $B_{\parallel}^{\star}$ denotes the Jacobian, $\boldsymbol{\kappa}$ is the curvature of the magnetic field $\mathbf{B}$ with magnitude B, and ρ is the mass density of the plasma. The particle mass and charge are denoted by m and Ze, respectively. Finally, $\mathrm{d}\Gamma$ indicates the integration over all of phase space. Note that the electrostatic potential (and similarly the parallel vector potential) is written as $\phi(\mathbf{r},t) = \hat{\phi}(t)\phi_0(\mathbf{r})\exp(\mathrm{i}\omega t)$. The damping rate γ_d, describing continuum, radiative, and Landau damping, is a free parameter of the model. The choice of γ_d is outlined in Ref. [3].

The collision operator

$$\mathcal{C}(f) = \nu_{\mathrm{D}}^{\mathrm{fi}}\mathcal{L}(f) + \frac{1}{v^2}\frac{\partial}{\partial v}\left[v^3\frac{m_\mathrm{f}}{m_\mathrm{f}+m_\mathrm{i}}\nu_{\mathrm{s}}^{\mathrm{fi}}f\right] + \frac{1}{v^2}\frac{\partial}{\partial v}\left[v^3\frac{m_\mathrm{f}}{m_\mathrm{f}+m_\mathrm{e}}\nu_{\mathrm{s}}^{\mathrm{fe}}f\right] \tag{7}$$

used in this paper is a fast-ion collision operator that describes pitch-angle collisions with the background ions (the first term, $\mathcal{L}$, is the Lorentz operator) and friction with the entire background plasma (second and third term), respectively. In Eq. (7), ν_D labels the deflection frequency and ν_s is the slowing-down frequency. Energy diffusion is neglected. The labels $\mathrm{i}, \mathrm{e}, \mathrm{f}$ are used to denote ions, electrons, and fast ions, respectively.

This collision operator is the same as the one used in Ref. [3]. The implementation of the Lorentz operator into the electromagnetic version of EUTERPE has been benchmarked in Ref. [9] and was used for non-linear simulations in Ref. [7].

3. Modes

As in Ref. [3], we investigate a W7-X high-mirror equilibrium with plasma profiles as expected for the 2018 experimental campaign. In this magnetic configuration, five different AEs are studied, which are possible candidates to be destabilized by fast ions generated by the NBI system. The same modes have been investigated in Ref. [3], with the focus on the linear growth rates and non-linear saturation levels. Ref. [3] showed that the fast-ion drive could be insufficient

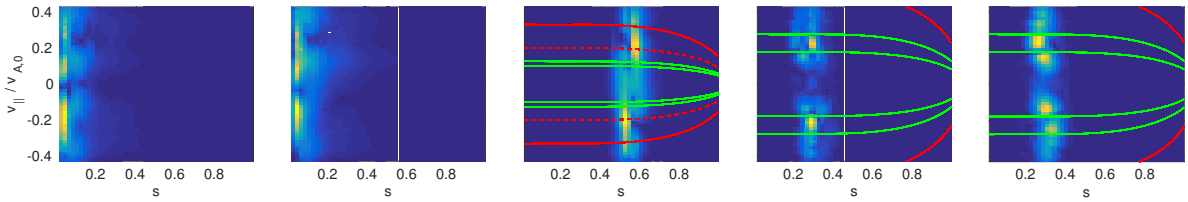

Figure 2. Absolute value of the wave-particle power transfer (arb. units) in the s-$v_\parallel$-plane for the modes shown in Fig. 1. The power transfer is strong where the gradient of the mode is large. The toroidal and helical resonances are shown as solid red and green lines for the gap modes. As shown for the TAE, the higher-order resonances (dashed red line) can play an important role.

to destabilize those modes. However, also the background plasma may contribute to the drive of the mode [10].

The radial mode structures are shown in Fig. 1. We study GAEs, EAEs, and a TAE. The latter two are gap modes (little continuum damping), but the GAEs could be subject to continuum damping. They are nevertheless added to our investigation, because they are expected to be easily destabilized in W7-X plasmas [11]. Since they fulfil $|m| = |n|$, they are called Isomon modes in Ref. [11].

4. Power transfer

It can be seen in Fig. 1 that especially the GAEs have a broad radial mode structure. In order to assess at which spatial position the drive is strongest, we investigate the wave-particle power-transfer in the s-$v_\parallel$-plane (integrating over poloidal and toroidal angle, and the magnetic moment). The results are shown in Fig. 2 for the same modes that were presented in Fig. 1. For the narrow gap modes, the drive is localized at the same radial position as the mode itself, which is expected. The broad GAEs, on the other hand, are not uniformly driven over their entire extent. Rather, the power transfer is restricted to a region where the mode structure exhibits the largest gradient. Comparing with Eq. (5), this is the expected behaviour.

In Fig. 2, the resonances (toroidal and helical Fourier components of the background magnetic field) are shown as solid red and green lines. They can be computed using

$$\frac{v_\parallel}{v_{\mathrm{A},\star}} = \left| 1 \pm 2 \frac{\iota_\star - \nu N}{\mu_0 \iota_\star - \nu_0 N} \right|^{-1} \tag{8}$$

for the well-localized gap modes [12]. Eq. (8) is not applicable to the GAEs, since for them a local approximation fails. Here, ι is the rotational transform, N denotes the number of field periods, μ_0, ν_0 determine the mode coupling, and ν relates to either the toroidal or helical resonance. Values that have to be taken at the mode localization region are indicated by a star.

For the TAE, the agreement with the simulated power transfer is not perfect. A possible explanation is that the drive could also come from higher-order resonances. This is shown for the TAE (middle plot), where the $v_\parallel/v_\mathrm{A} = 1/5$ resonance (dashed red line) is found to agree well with the simulation.

It needs to be pointed out that the destabilization of the EAEs is particular to W7-X being a stellarator. The usual tokamak resonance of $v_\parallel/v_\mathrm{A} = 1/2$ is not reached. Only the helical structure of the magnetic field provides additional resonances at lower velocities.

5. Growth rates in helium plasmas

While previous operation phases of W7-X relied on helium plasmas for high-density operation the 2018 experimental campaign will feature mostly hydrogen plasmas. There are however

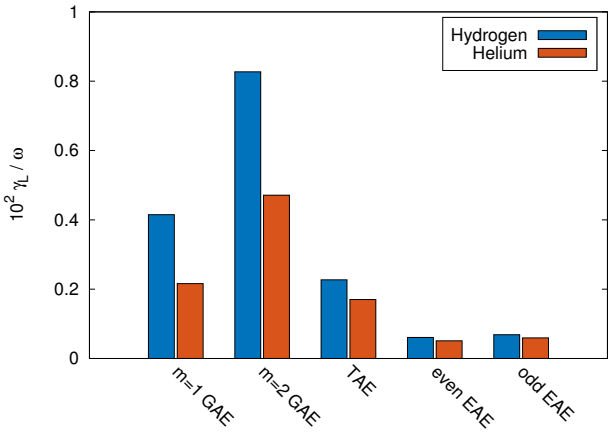

Figure 3. Linear growth rates (for $\gamma_d = 0$) of the five AEs shown in Fig. 1 normalized to their respective mode frequency. Lower normalized growth rates are observed in helium plasmas. The composition of the background plasma more strongly influences the low-frequency GAEs than the high-frequency EAEs.

proposals to study the effects of the background-plasma mass density on Alfvén-wave activity.

Fig. 3 shows the linear growth rates of the five AEs shown in Fig. 1 normalized to their respective mode frequency for hydrogen as well as helium plasmas. The fast ions injected into those plasmas are always protons. It can be seen that the normalized growth rates are generally reduced in helium plasmas. This effect is most pronounced for the GAEs. The EAEs, on the other hand, are barely influenced.

The reduction of the normalized growth rates in helium plasmas can be explained by a shift of the resonances. Given the injection parameters of the NBI system, at most $v_\parallel/v_A \approx 0.43$ can be reached for hydrogen. Taking the TAE as an example, $v_\parallel/v_A = 1/3$ and $v_\parallel/v_A = 1/5$ (higher-order resonance) are included, but the primary $v_\parallel/v_A = 1$ resonance is not. If helium is used instead, the Alfvén velocity drops, and the $v_\parallel/v_A = 1$ resonance becomes almost reachable. This mechanism would increase the drive in a tokamak. In a stellarator, however, the magnetic field also has helical Fourier harmonics, which in W7-X are larger than the toroidal Fourier harmonic. The additional helical resonances modify the shape of the resonance curve [13, 14]

$$\frac{\gamma}{\omega} \sim \sum_{j=\pm 1} \left[\epsilon_t^2 F\left(w_t^{(j)}\right) + \epsilon_h^2 F\left(w_h^{(j)}\right) \right] \tag{9}$$

$$F = w\left(1 + 2w^2 + 2w^4\right) \exp\left[-w^2\right] \tag{10}$$

so that the modes are more stable in helium than they are in hydrogen. Here, w is the resonant velocity and ϵ_t and ϵ_h denote the toroidal and helical Fourier components of the magnetic field, respectively.

This finding suggests that hydrogen plasmas could be more suitable for observing AE activity in W7-X in up-coming experimental campaigns.

6. The influence of collisions

It was reported in the past (see e.g. Refs. [7, 15, 16]) that collisions can influence the non-linear saturation levels of AEs. The fast-ion collision operator used here includes the effects of pitch-angle scattering and drag. In order to disentangle their contributions to the non-linear saturation, we vary the strength of both terms individually for the $m = 2$ GAE and the TAE. The results can be seen in Figs. 4 and 5, respectively. Both figures confirm the potentially strong influence of collisions on the saturation level. For the GAE, a 50% increase is possible. For the TAE, it is even possible to increase δB^{sat} (value of δB at the first maximum) by a factor of approximately 10. This emphasizes the tremendous importance of having a fast-ion collision operator present in non-linear simulations. At the radial position where the TAE is localized,

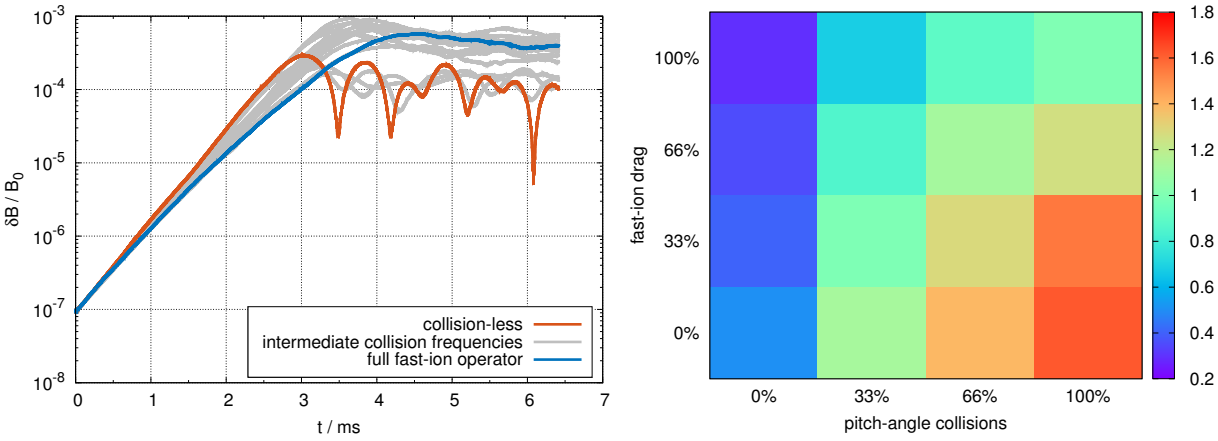

Figure 4. Time trace of the perturbed poloidal magnetic field of the $m = 2$ GAE for various strengths of the fast-ion collision operator (left). The right-hand side shows the value of $\delta B/B_0$ at saturation (normalized to the saturation level including the full collision operator) in colour code. Pitch-angle collisions increase the saturation level, while fast-ion drag lowers it.

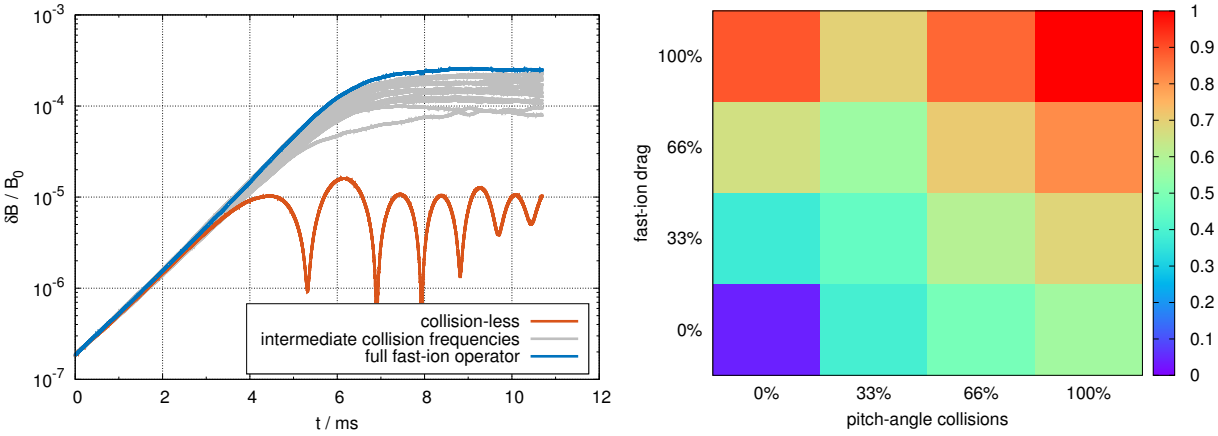

Figure 5. Same as Fig. 4, but for the TAE. Contrary to Fig. 4 ($m = 2$ GAE) both pitch-angle collisions and fast-ion drag increase the saturation level.

the basic collision frequencies (see Ref. [17] for their definition and relation to ν_D and ν_s) are $\nu_0^\mathrm{fi} = 48.8\ \mathrm{s}^{-1}$ and $\nu_0^\mathrm{fe} = 38.3\ \mathrm{s}^{-1}$.

Fast-ion drag and pitch-angle scattering are found to act differently on different AEs. In case of the GAE, there is a clear division: Pitch-angle scattering increases the saturation level while fast-ion drag lowers it, which means that the highest saturation level is not achieved with the self-consistent collision operator. The role of drag is different for the TAE, where it also acts to increase δB^sat. There seems to be a synergy between pitch-angle scattering and fast-ion drag, which is weakest at intermediate values of the pitch-angle collision frequency. The highest saturation level is obtained with the full fast-ion collision operator.

Pitch-angle scattering counteracts wave-particle trapping [15], the mechanism for saturation [15, 18], and thus allows for a higher saturation level. For the TAE, fast-ion drag has a similar effect. It needs to be pointed out that the radial positions of the $m = 2$ GAE and TAE are different. In this realistic scenario the density and temperature profiles are not flat, which makes the collision frequencies strong functions of the radial position. This could explain why fast-ion

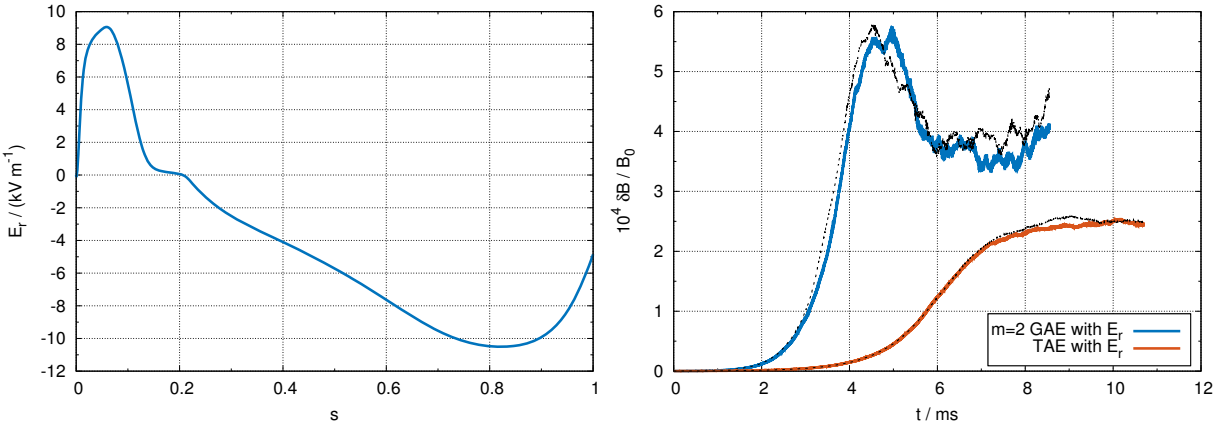

Figure 6. Radial structure of the radial electric field as determined by NTSS [19] calculations consistent with the input plasma profiles (left). On the right: E_r slightly modifies the non-linear dynamics of the TAE mode. The $m = 2$ GAE is also influenced in the linear phase. For reference, the black dashed lines are the cases without E_r. Overall, the impact of a radial electric field is very small.

drag acts differently on the two AEs. Another possibility is that the behaviour is due to the differences in the resonances.

7. The influence of a radial electric field

We would also like to investigate the impact of a radial electric field on the non-linear dynamics of the $m = 2$ GAE and the TAE. Here, we combine the calculations including E_r with the fully self-consistent fast-ion collision operator in order to progress to a more realistic case. Note however that the $\mathbf{E} \times \mathbf{B}$ Doppler shift of the mode frequency and a possible change of the MHD mode structure due to the radial electric field are neglected. Here, we just retain the influence of E_r on the particle motion. A more accurate treatment will be left for future work.

The radial shape of E_r is shown in Fig. 6 on the left-hand side. Over a wide radial range the radial electric field is negative (ion root). In the core, however, the radial electric field is positive, which corresponds to electron-root conditions. This is characteristic for low-plasma-density discharges in first operation phases of W7-X, in which core-localized electron heating usually dominates. The radial electric field leads via the $\mathbf{E} \times \mathbf{B}$-drift to a further modification of the particle trajectories. This could potentially alter the wave-particle trapping mechanism and thus influence the saturation. How a radial electric field influences fast-ion-driven AEs has been considered in the past [20] for linear simulations. Here, we also consider the non-linear development of the mode.

The right-hand side of Fig. 6 shows the non-linear development of the amplitudes of the $m = 2$ GAE and of the TAE, respectively. Simulations including E_r are shown as solid lines, the ones without the radial electric field as black dashed lines. The figure shows that the saturation level stays nearly identical. (The other modes shown in Fig. 1 are found to behave similarly.) The linear growth rate reduces by 5% for the $m = 2$ GAE if the radial electric field is included. Overall, the impact of E_r on the mode dynamics is very small.

8. Summary and Conclusions

In this paper we studied several possible actuators that could be of experimental relevance for finding (or avoiding) operational conditions that show Alfvén-wave activity in Wendelstein 7-X (W7-X). Among the actuators investigated are the composition of the background plasma

(hydrogen vs. helium), fast-ion collisions, and the presence of a radial electric field. The present paper can be viewed as a continuation of Ref. [3] with the aim of testing the sensitivity of the results to the specifics of the input.

Five different Alfvén eigenmodes (AEs) in a W7-X high-mirror configuration were investigated. They are driven unstable by fast ions generated by neutral beam injection. The fast-ion density profile and distribution function in energy space were computed using the ASCOT code [4, 5]. The profiles of the background plasma were calculated by NTSS [19] for plasmas expected in the 2018 operational campaign of W7-X.

When looking at the power transfer in phase space, we saw that for the gap modes the drive comes from regions where the mode is localized. For the GAEs, the region of the drive coincides with the strongest gradient of the mode. We found that, due to the limited injection energy of the fast ions, EAEs can only be excited via the helical couplings present in a stellarator such as W7-X.

We also showed that the normalized growth rates of all AEs are lower in helium than in hydrogen. This could be explained by a shift of the resonances coupled with the existence of stellarator-specific helical Fourier components in W7-X. This result indicates that hydrogen plasmas might be a better candidate for observing AE activity. Furthermore, we could confirm that the role of the fast-ion collision operator is different for different AEs. Fast-ion drag increases the saturation level for the TAE, but decreases it for the $m = 2$ GAE. Since the collision frequencies are a strong function of density and temperature, this is a mechanism which could select a specific AE to be visible in specific experimental conditions. Finally, the role of a radial electric field was investigated. We found that for the specific case looked at, the presence of E_r does not affect the non-linear dynamics significantly. This may change if the full effect of the radial electric field is taken into account in CKA, which we plan for the future.

All simulations were carried out using the CKA-EUTERPE model [6]. It is a perturbative model that does not include fast-ion-induced mode-structure modifications. But since the fast-ion beta is low, such an approach seems justified. In a future work, the present results should nevertheless be compared to a fully gyro-kinetic simulation.

Acknowledgments

This work has been carried out within the framework of the EUROfusion Consortium and has received funding from the Euratom research and training programme 2014-2018 under grant agreement No 633053. The views and opinions expressed herein do not necessarily reflect those of the European Commission.

The simulations were performed on the MARCONI supercomputer (CINECA).

References

[1] Heidbrink W W 2008 *Phys. Plasmas* **15** 055501
[2] Duong H H, Heidbrink W W, Strait E J, Petrie T W, Lee R, Moyer R A and Watkins J G 1993 *Nucl. Fusion* **33** 749–765
[3] Slaby C, Könies A, Kleiber R, Äkäslompolo S and Kontula J 2018 *Europhysics Conference Abstracts* **42A** P4.1098 URL `http://ocs.ciemat.es/EPS2018PAP/pdf/P4.1098.pdf`
[4] Heikkinen J A and Sipilä S K 1995 *Phys. Plasmas* **2** 3724–3733
[5] Hirvijoki E, Asunta O, Koskela T, Kurki-Suonio T, Miettunen J, Sipilä S, Snicker A and Äkäslompolo S 2014 *Comput. Phys. Commun.* **185** 1310–1321
[6] Fehér T B 2013 *Simulation of the interaction between Alfvén waves and fast particles* Ph.D. thesis Ernst-Moritz-Arndt-Universität Greifswald
[7] Slaby C, Könies A, Kleiber R and García-Regaña J M 2018 *Nucl. Fusion* **58** 082018
[8] Könies A et al 2018 in preparation
[9] Slaby C, Kleiber R and Könies A 2017 *Comput. Phys. Commun.* **218** 1–9
[10] Könies A, Mishchenko A and Hatzky R 2008 *Theory of Fusion Plasmas* vol 1069 ed Garbet X, Sauter O and Sindoni E (New York: American Institute of Physics) pp 133–143

[11] Kolesnichenko Y I, Könies A, Lutsenko V V, Drevlak M, Turkin Y and Helander P 2016 *Nucl. Fusion* **56** 066004
[12] Kolesnichenko Y I, Lutsenko V V, Wobig H and Yakovenko Y V 2002 *Nucl. Fusion* **42** 949–958
[13] Fu G Y and Dam J W V 1989 *Phys. Fluids B* **1** 1949–1952
[14] Kolesnichenko Y I, Lutsenko V V, Wobig H and Yakovenko V 2002 *Phys. Plasmas* **9** 517–528
[15] Berk H L, Breizman B N and Huanchun Y 1992 *Phys. Rev. Lett.* **68** 3563–3566
[16] Lang J, Fu G and Chen Y 2010 *Phys. Plasmas* **17** 042309
[17] Helander P and Sigmar D J 2002 *Collisional Transport in Magnetized Plasmas* (Cambridge University Press)
[18] Briguglio S, Wang X, Zonca F, Vlad G, Fogaccia G, Troia C D and Fusco V 2014 *Phys. Plasmas* **21** 112301
[19] Turkin Y, Beidler C D, Maaßberg H, Murakami S, Tribaldos V and Wakasa A 2011 *Phys. Plasmas* **18** 022505
[20] Mishchenko A, Könies A, Fehér T, Kleiber R, Borchardt M, Riemann J, Hatzky R, Geiger J and Turkin Y 2014 *Nucl. Fusion* **54** 104003